Chapter 1
Introduction to Metamaterials

In this chapter, we start with a brief discussion on the origins of metamaterials, and their basic electromagnetic and optical properties. We then present some metamaterial structures and potential applications in areas such as sub-wavelength imaging, antenna design, invisibility cloak, and biosensing. After all these, we then move to the related mathematical problems by introducing the governing equations used to model the wave propagation in metamaterials. Finally, a brief overview of some popular computational methods for solving Maxwell's equations is provided.

1.1 The Concept of Metamaterials

The prefix "meta" means "beyond," and in this sense the terminology "metamaterials" implies artificially structured composite materials consisting of unit cells much smaller than the wavelength of the incident radiation and displaying properties not usually found in natural materials. More specifically, we are interested in a metamaterial with simultaneously negative electric **permittivity** ϵ and magnetic **permeability** μ. In general, both permittivity ϵ and permeability μ depend on the molecular and perhaps crystalline structure of the material, as well as bulk properties such as density and temperature.

Back in 1968, Russian physicist Victor Veselago wrote a seminar paper [288] on metamaterials (he then called left-handed materials). In that paper, he speculated that the strikingly unusual phenomena could be expected in a hypothetical left-handed material in which the electric field **E**, the magnetic field **H** and the wave vector **k** form a left-handed system. The paper explicitly presented that to achieve such a left-handed material, the required material parameters should be simultaneously negative for both permittivity and permeability. However, due to the non-existence of such materials in nature, Veselago's paper did not make a big impact until the first successful construction of such a medium by Smith et al. in 2000 [271], and the first experimental demonstration of the negative refractive

J. Li and Y. Huang, *Time-Domain Finite Element Methods for Maxwell's Equations in Metamaterials*, Springer Series in Computational Mathematics 43,
DOI 10.1007/978-3-642-33789-5_1, © Springer-Verlag Berlin Heidelberg 2013

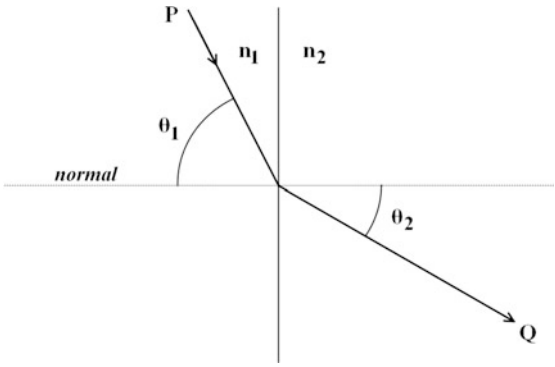

Fig. 1.1 Demonstration of Snell's law

index in 2001 [260]. Another catalyst was caused by Pendry's landmark work on perfect lens [234], which sparked the attempt to consider metamaterials for many potentially exciting applications. According to [274, p. 317], these four seminar papers together made the birth of the subject of metamaterials. Since 2000, there has been a tremendous growing interest in the study of metamaterials and their potential applications in areas ranging from electronics, telecommunications to sensing, radar technology, sub-wavelength imaging, data storage, and design of invisiblity cloak.

1.1.1 Basic Electromagnetic and Optical Properties

The optical properties of many materials can be characterized by the so-called **refractive index** (or index of refraction) n, which is defined as

$$n = \frac{c}{v}, \tag{1.1}$$

where c and v denote the speeds of light in vacuum and in the underlying material, respectively. This definition represents the optical density of the underlying medium. Hence for a normal medium, the number n is typically greater than one.

The refractive index n is often seen in the Snell's law (see Fig. 1.1):

$$n_1 \sin\theta_1 = n_2 \sin\theta_2, \tag{1.2}$$

which states that the ratio of the sines of the angles of incidence and refraction is equivalent to the reciprocal ratio of the refraction indices in two different isotropic media. Here θ_1 and θ_2 denote the incidence angle and refraction angle, respectively.

The refractive index n can also be defined using the well-known Maxwell relation

$$n = \sqrt{\epsilon_r \mu_r}. \tag{1.3}$$

This relation connects the refractive index n, an optical quantity, with two electromagnetic quantities: the permittivity ϵ_r and permeability μ_r of a medium relative to the permittivity ϵ_0 and permeability μ_0 in vacuum. Note that $\epsilon_0 = \epsilon/\epsilon_r = 8.854{\cdot}10^{-12}\,\mathrm{N/A^2}$ and $\mu_0 = \mu/\mu_r = 4\pi{\cdot}10^{-7}$ force/m. It is know that vacuum has a refractive index of 1, and the speed of light in vacuum $c = 1/\sqrt{\epsilon_0\mu_0} \approx 3\times10^8$ m/s.

One important concept in study of wave propagation problems is **phase velocity**, which is the rate at which the phase of the wave propagates in space. This is the speed at which the phase of any one frequency component of the wave travels. Mathematically, the phase velocity v_p is defined as the ratio of the wavelength λ (the distance between any two points with the same phase, such as between crests, or troughs) to period T (measured in seconds), i.e.,

$$v_p = \frac{\lambda}{T},$$

which can also be represented as

$$v_p = \frac{\omega}{k}, \tag{1.4}$$

where $\omega \equiv \frac{2\pi}{T}$ is the wave's angular frequency (measured in radians per second), and $k \equiv \frac{2\pi}{\lambda}$ is the angular wavenumber.

Another important concept in wave propagation is **group velocity**, which is used to describe the velocity with which the overall shape of the wave's amplitudes (known as the modulation or envelope of the wave) propagates through space. Mathematically the group velocity v_g is defined as

$$v_g = \frac{\partial\omega}{\partial k}. \tag{1.5}$$

The function $\omega = \omega(k)$ is known as the dispersion relation. If ω is directly proportional to k, then the group velocity is exactly equal to the phase velocity. Otherwise, the group velocity will behave very differently from the phase velocity. For example, in a dispersive medium (in which the phase velocity of a wave depends on frequency), the envelope of the wave packet become distorted as the wave propagates, since waves with different frequencies move at different speeds.

From (1.4) and (1.5), we can relate the group velocity to the phase velocity as follows:

$$\frac{1}{v_g} = \frac{1}{v_p} + \omega\frac{\partial}{\partial\omega}\left(\frac{1}{v_p}\right). \tag{1.6}$$

In the normal dispersion case, $\frac{\partial}{\partial\omega}(\frac{1}{v_p}) > 0$ implies that $v_g < v_p$. Under this situation, the group velocity is often thought of as the velocity at which energy or information is conveyed along a wave. However, if the wave travels through

an absorptive medium, this does not always hold. For example, in the anomalous dispersion, $\frac{\partial}{\partial\omega}(\frac{1}{v_p}) < 0$ implies that $v_g > v_p$. A real application of this fact is that laser light pulses are sent through specially prepared materials in order to have the group velocity significantly exceed the speed of light in vacuum. It is also possible to reduce the group velocity to zero, which makes the pulse immobile; or to have a negative group velocity, which makes the pulse appear to propagate backwards. In these cases, the group velocity loses its usual meaning as the transfer velocity of energy or information.

For isotropic double negative metamaterials, Veselago [288] showed that the phase velocity would be antiparallel to the direction of the energy flow, which is contrary to wave propagation in natural materials. This fact can be justified as follows. Let us denote the Poynting vector

$$\mathbf{S} = \frac{1}{2}\mathrm{Re}(\mathbf{E} \times \mathbf{H}^*),$$

where the star denotes complex conjugate. The Poynting vector $\mathbf{S}$ gives the magnitude and direction of power flow. Assume a plane wave propagating in a medium as

$$\mathbf{E} = \tilde{\mathbf{E}} e^{j(\omega t - \mathbf{k}\cdot\mathbf{r})}, \quad \mathbf{H} = \tilde{\mathbf{H}} e^{j(\omega t - \mathbf{k}\cdot\mathbf{r})}, \tag{1.7}$$

where $j = \sqrt{-1}$ is the imaginary unit, then substituting (1.7) into Maxwell's equations (1.9) and (1.10) given below in Sect. 1.2 with the constitutive relations (1.11), we have

$$\epsilon\omega\tilde{\mathbf{E}} = -\mathbf{k} \times \tilde{\mathbf{H}}, \quad \mu\omega\tilde{\mathbf{H}} = \mathbf{k} \times \tilde{\mathbf{E}}, \tag{1.8}$$

which shows that: If ϵ and $\mu > 0$, then vectors $\tilde{\mathbf{E}}$, $\tilde{\mathbf{H}}$ and $\mathbf{k}$ obey the right-hand rule; If ϵ and $\mu < 0$, then vectors $\tilde{\mathbf{E}}$, $\tilde{\mathbf{H}}$ and $\mathbf{k}$ obey the left-hand rule, i.e., $\mathbf{S}$ and $\mathbf{k}$ have opposite directions.

Hence, if we assume that the energy flux moving away from the source is the positive direction as usual, then the phase velocity of a propagating wave in a metamaterial points towards the source. For this reason and the definition of $n = c/v$, metamaterials could be considered as having a negative refractive index, i.e.,

$$n = -\sqrt{\epsilon_r \mu_r}, \quad \text{when } \epsilon_r < 0,\ \mu_r < 0.$$

One striking property for metamaterials is the so-called re-focusing property. Let us assume that a line source is placed $\frac{d}{2}$ before a metamaterial slab with width d and refractive index $n_r = -1$, the medium outside the slab is free space (i.e., $n_i = 1$). By Snell's law (1.2), the refraction angle θ_r is equal to the negative incidence angle θ_i. Hence all rays emanating from the line source will be refocused inside the metamaterial slab and have another focus at the back of the slab (see Fig. 1.2).

Another interesting property for metamaterials is that the Doppler effect (or Doppler shift) in metamaterials is reversed. Recall that the well-known Doppler effect tells us that: For wave propagating in a standard medium (such as sound wave in air), the wave frequency increases for an observer as the source of the wave moves

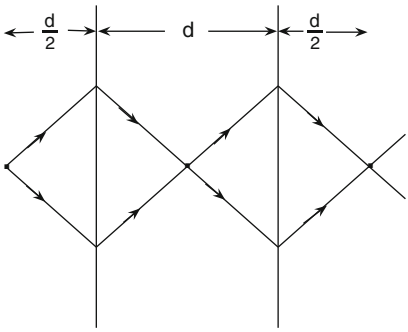

Fig. 1.2 Demonstration of the refocusing property

closer; while the wave frequency decreases for the observer as the source of the wave moves away. A simple example of Doppler effect is that when an ambulance approaches, the sound wave generated from its siren is compressed, which increases the wave frequency or pitch; when the ambulance moves away, the sound wave is stretched, which causes the siren's pitch to decrease. On the other hand, for the electromagnetic wave propagating in a metamaterial, the wave frequency decreases for an observer as the wave source moves closer. This can be very scary. Just imagine that if the air were filled with metamaterials, then a missile could reach the target without any awareness.

1.1.2 Basic Structures

The first double negative metamaterial was constructed by a group of physicists at the University of California at San Diego led by David Smith et al. [271]. The material consists of a two-dimensional array of repeated unit cells of square copper split ring resonators (SRRs) and copper wire strips on fiber glass circuit board. The SRR is made of two concentric rings separated by a gap, and both rings have splits at opposite sides, see Fig. 1.3. By careful design of the split width, gap distance, metal width and radius, the SRR can hopefully create a strong magnetic resonance which leads to negative permeability μ. While the metal wire is used to provide the negative permittivity ϵ by carefully choosing the distance between the wires and the size of their cross section. Experiments carried out by Shelby et al. [260] demonstrate that this structure shows negative refraction index and left-handed behavior for incident plane waves with electric field polarized parallel to the continuous wire and magnetic field perpendicular to the SRR.

Various modifications of SRRs have been proposed in the literature, aiming mainly to make the structure easy to fabricate, reduce the overall size of the cell element, and reduce the loss of the structure. For example, a set of split ring resonators was investigated by Aydin et al. [15]. Their constructions are shown in

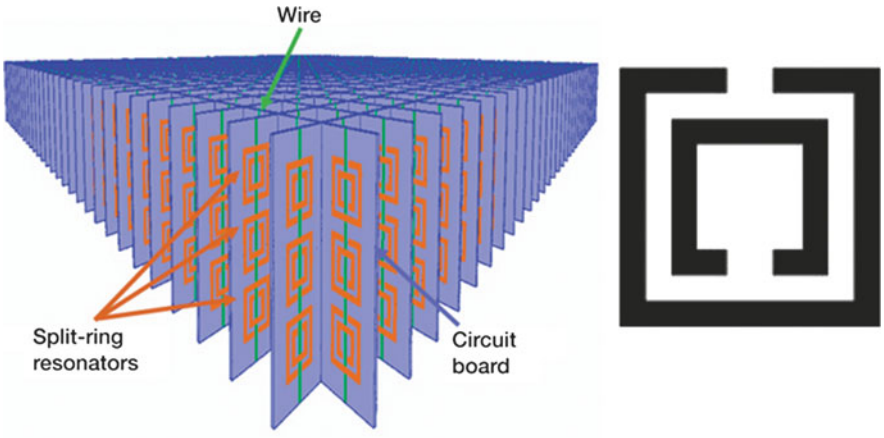

Fig. 1.3 (*Left*): An exemplary metamaterial formed by square split ring resonators (SRRs) and metal wires (Source: http://en.wikipedia.org/wiki/File:Left-handed_metamaterial_array_configuration.jpg) (Author: Cynthia.L.Dreibelbis@nasa.gov). (*Right*): A unit cell of square split ring resonators (SRRs)

Fig. 1.4 Some split ring resonators designed by Aydin et al. [15] (Reproduced with permission from Fig. 11 of [15])

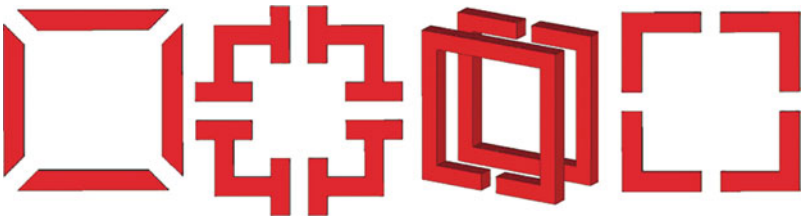

Fig. 1.5 Some split ring resonators studied by Kafesaki et al. [164] (Reproduced with permission from Fig. 16 of [164])

Fig. 1.4. The first three are single rings split one, two and four times, respectively. The fourth and fifth are double rings split four and eight times, respectively.

In 2005, Kafesaki et al. [164] carried out a comprehensive numerical study of many SRRs (see Fig. 1.5). They studied the magnetic and the electric response of single-ring and double-ring SRRs, and how the responses of SRRs depend on the length, width and depth of the metallic sides for different kinds of SRRs.

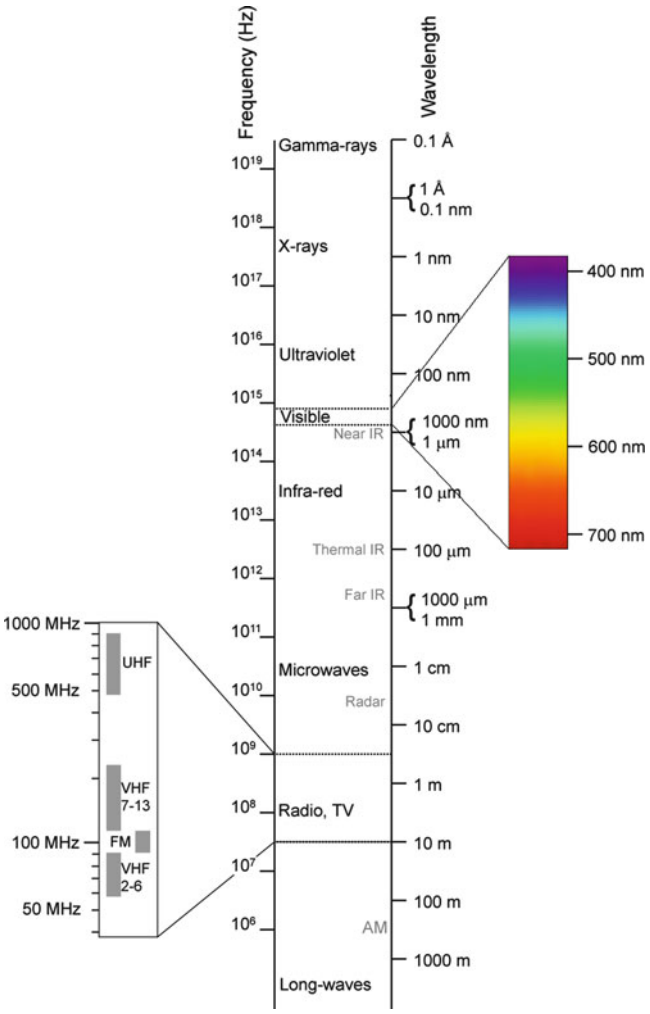

Fig. 1.6 The whole electromagnetic spectrum (Source: http://en.wikipedia.org/wiki/Electromagnetic_spectrum)

Recently, in search of higher-frequency resonators, researchers found that the resonant frequency saturates as the SRR size becomes smaller and smaller. Extension of metamaterials based on split ring resonators to near-infrared and visible wavelengths (the whole electromagnetic spectrum is shown in Fig. 1.6) becomes quite challenging and often involves difficult fabrication problem. A popular structure in optical wavelengths is a fishnet design, which consists of a metal-dielectric-metal sandwich. A square array of holes riddles the sandwich, which makes the structure similar to a real fishnet. The holes may be circular, elliptical or rectangular.

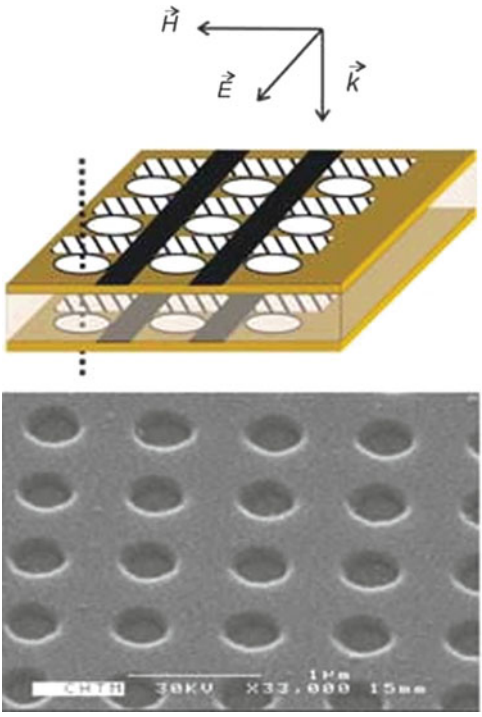

Fig. 1.7 (*Top*): A multilayer fishnet structure designed by Zhang et al. [301, Fig. 1]. (*Bottom*): The scanning electron microscopy (SEM) picture of the fabricated structure (Reprinted with permission from Zhang et al. [301]. Copyright (2005) by the American Physical Society)

Figure 1.7 shows a multilayer fishnet structure designed by Zhang et al. [301]. It consists of an Al_2O_3 dielectric layer between two Au films perforated with a square periodic array of circular holes (period 838 nm; hole diameter is about 360 nm) atop a glass substrate.

In [285], Valentine et al. experimentally demonstrated the first 3-D fishnet metamaterial (see Fig. 1.8), which is fabricated on a multilayer metal-dielectric stack. This structure consists of alternating layers of 30 nm silver (Ag) and 50 nm magnesium fluoride (MgF_2).

All the structures mentioned so far have anisotropic properties. To construct an isotropic metamaterial, the unit cell should have some symmetries. Some 3-D isotropic resonators have been proposed [124, 232, 236]. One example is shown in Fig. 1.9.

1.1.3 Potential Applications

1.1.3.1 Subwavelength Imaging

It is known that conventional lens-based imaging devices cannot provide resolution better than $\lambda/2$, where λ is the radiation wavelength. Such restriction is the

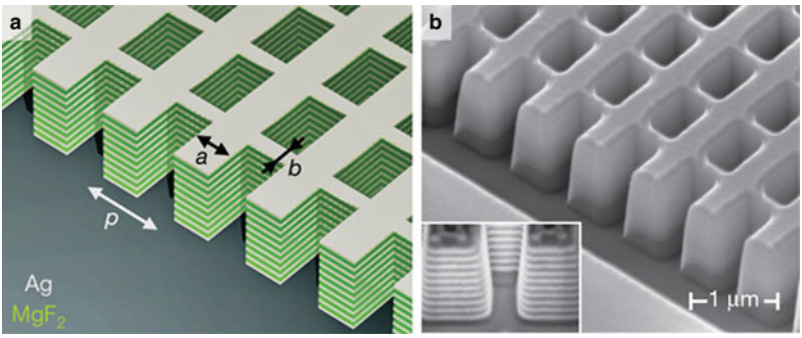

Fig. 1.8 (*Left*): The 21-layer fishnet structure designed by Valentine et al. [285, Fig. 1]. The dimensions of the unit cell are $p = 860$ nm, $a = 565$ nm (width of wide slabs) and $b = 265$ nm (width of thin slabs). The structure consists of alternating layers of 30 nm silver (Ag) and 50 nm magnesium fluoride (MgF2), (*Right*): The SEM image of the 21-layer fishnet structure with the side etched, showing the cross-section (Reprinted by permission from Macmillan Publishers Ltd: Nature [285], copyright (2008))

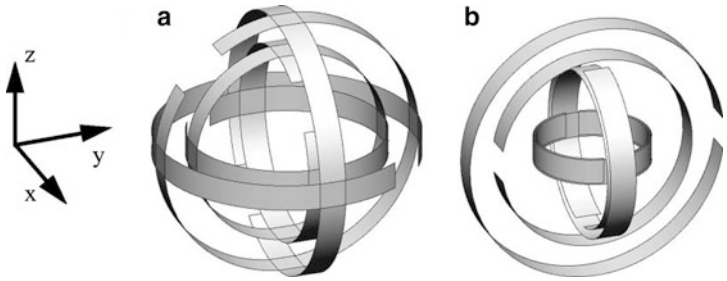

Fig. 1.9 3D isotropic resonators: Gay-Balmaz et al.'s design [124, Fig. 6]. (**a**) The structure is built from three identical SRRs normal to each other. (**b**) The structure is composed of three SRRs of increasing size (Reprinted with permission from Gay-Balmaz and Martin [124]. Copyright (2002), American Institute of Physics)

so-called diffraction limit. In recent years, several techniques based on the use of metamaterials have been proposed for subwavelength imaging in different ranges of electromagnetic spectrum. Proposed techniques include perfect lens [234], silver superlenses [116], hyperlenses [205, 221, 272], and wire medium lenses [265, 266].

For example, Silveirinha et al. [265] showed that a wire medium lens made of silver nanorods could achieve subwavelength resolution of $\lambda/10$ at 33 THz. Figure 1.10 presents the results of [265].

Another interesting example was proposed by Fang et al. [116]. An object "NANO" with 40 nm linewidth was imaged by silver superlens. The object was clearly imaged even when the incoming wave had 365 nm wavelength, which means that $\lambda/9$ image resolution was obtained.

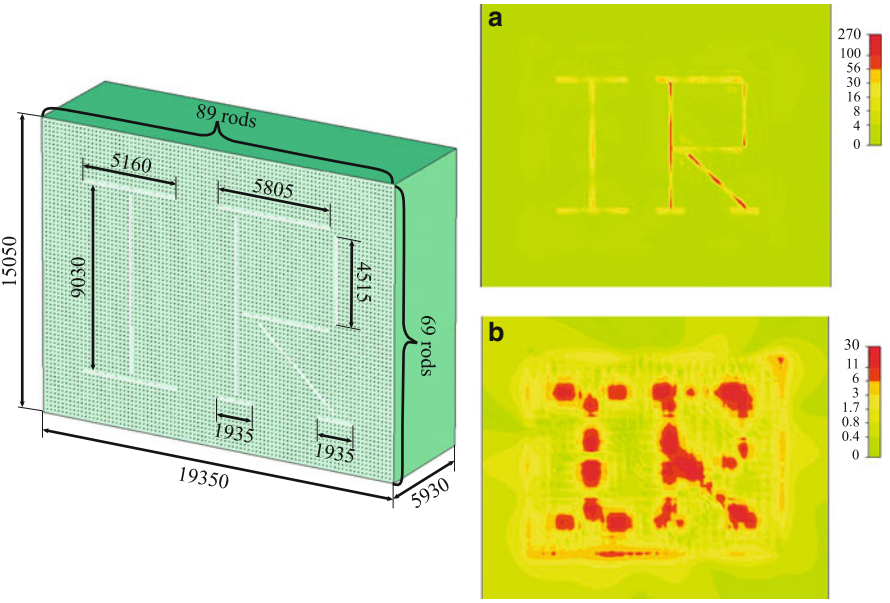

Fig. 1.10 (*Left*): The setup of the imaging simulation, where the numbers are in nm. (*Right*) Distributions of $|E_z|$ at 33 THz at the source plane (*Top*) and image plane (*Bottom*) (Source: Reprinted with permission from Silveirinha et al. [265]. Copyright (2007) by the American Physical Society)

1.1.3.2 Circuit Applications

Due to the small dimensions of SRRs and complementary split ring resonators (CSRRs, a dual of SRR by switching metal and air) relative to the signal wavelength at their resonance frequency, SRR and CSRR-based transmission lines are useful for device miniaturization. Applications in microwave passive components such as impedance inverters, power dividers [257], couplers, and filters have been discussed. SRRs are also useful particles in many other applications such as magnetoinductive and electroinductive wave components [37, 275], frequency selective surfaces [18].

1.1.3.3 Antenna Applications

Recently, researchers have proposed some methods to obtain miniaturized antennas made of ideal homogenized metamaterials. The first design of a subwavelength antenna with metamaterials for the case of dipole and monopole radiators was proposed by Ziokowski's group [312]. The basic design consists of an electrically

short electric dipole (or monopole) surrounded by a double-negative (DNG) or an epsilon-negative (ENG) spherical shell with an electrically short radius. The compact resonance arises at the interface between the DNG (or ENG) shell and the free space. Similar ideas have been used to design subwavelength patch antennas [7, 38] and leaky-wave antennas [8].

1.1.3.4 Cloaking

Invisibility has long been a dream of human beings. Cloaking devices are advanced stealth technologies still in development that can make objects partially or wholly invisible to some portions of the electromagnetic spectrum.

Generally speaking, there are several major approaches to render objects invisible. For example, Alu and Engheta [6] proposed to use plasmonic coatings to cancel the dipolar scattering. But this technique is limited to the sub-wavelength scale of the object, and the coating depends on the geometry and material parameters of the object. Milton and Nicorovici [212] discovered that using a metamaterial coating would cloak polarizable line dipoles. But the coating is affected by the objects placed inside. Leonhardt [180] and independently Pendry, Schurig and Smith [237] discovered a coordinate transformation mechanism for electromagnetic cloaking. Their mechanism was quite similar to that of Greenleaf et al. [130, 131] introduced for conductivity. Their main idea is to guide electromagnetic wave around the cloaked region, and many later work has adopted this technique.

In May 2006, the first full wave numerical simulations on cylindrical cloaking was carried out by Cummer et al. [96]. A few months later, the first experiment of such a cloak at microwave frequencies was successfully demonstrated by Schurig et al. [254], where the cloak surrounding a 25-mm-radius Cu cylinder was measured.

After 2006, numerous studies have been devoted to cloaking, mainly inspired by [96, 254]. For example, in 2008, Liang et al. [197] performed a time-dependent simulation for the cylindrical cloak using finite-difference time-domain method. Their simulation (cf. Fig. 1.11) clearly shows the dynamical process of the electromagnetic wave in the cloaking structure. Figure 1.11 is obtained by considering only the E-polarized modes with permittivity and permeability components ϵ_z, μ_r and μ_θ satisfying the Lorentzian dispersive function $f_j(\omega) = \omega_p^2/(w_{aj}^2 - \omega^2 - j\omega\gamma)$, where $j = z, r, \theta$. The setup of the cloaking system is shown in Fig. 1.11a with R_1 and $R_2 = 2R_1$ as the inner and the outer cylindrical radii of the cloaking structure. A perfect electric conductor shell is put against the inner surface of the structure. An incident plane wave with frequency ω_0 moves form left side towards the cloaking structure, which is surrounded by the free space. As we can see, the cloaking effect is built up step by step. Finally, the field gets to the stable state shown in Fig. 1.11f, which clearly shows that the plane wave pattern gets recovered after the wave passes through the cloaking structure.

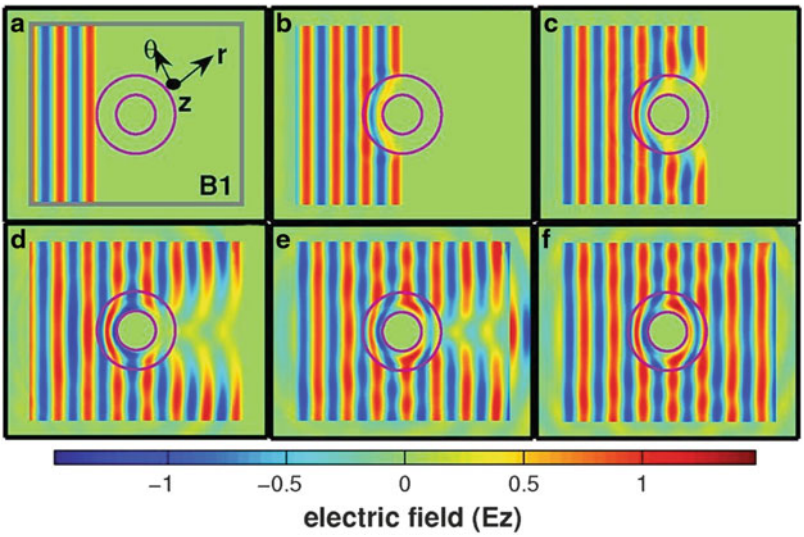

Fig. 1.11 The distribution of the electric field at different times: (**a**) $t = 2.28T$; (**b**) $t = 3.60T$; (**c**) $t = 4.92T$; (**d**) $t = 7.20T$; (**e**) $t = 9.00T$; (**f**) Stable state. T is the period of the incident wave (Reprinted with permission from Liang et al. [197]. Copyright (2008), American Institute of Physics)

1.1.3.5 Biosensing

Another potential application field of metamaterials is on biosensing. Conventional biosensors (such as those based on electro-mechanical transduction, fluorescence, nanomaterials, and surface plasmon resonance) often involve labor-intensive sample preparation and very sophisticated equipment.

In recent years, researchers have proposed to use metamaterials as candidates for detection of highly sensitive chemical, biochemical and biological analytes. For example, Lee et al. [177] studied the possibility of using split-ring resonators (SRRs) for biosensors. The basic principle is based on the fact that SRR can be considered to be a simple LC circuit with a response frequency of $f = 1/2\pi\sqrt{LC}$, which shows that the resonant frequency varies in terms of the changes in the inductance L and/or capacitance C. Hence the resonant frequency of SRR shall be shifted before and after the introduction of biomaterials.

Planar metamaterials were proposed to serve as thin-film sensors recently by O'Hara et al. [230]. They found that a resonant frequency response can be tuned through metamaterial designs. Though their metamaterial design can only detect thin films having a thickness less than 100 nm, their work presents a promising outlook for THz sensing technology.

1.1.3.6 Particle Detection

It is known that when charged particles move in a medium with velocity larger than $\frac{c}{n}$ (the phase velocity of light in the medium), Cherenkov radiation (CR) is emitted. Recall that c is the speed of light in vacuum, and n is the index of refraction of the medium. An example of CR is the blue glow seen in a nuclear reactor. Devices sensitive to Cherenkov radiation, called Cherenkov detectors, have been used extensively for detecting fast moving charged particles, and measuring the intensity of reactions etc.

Since the recently constructed metamaterials have negative refractive index, which results in the so-called reversed CR [288], a phenomenon can be used to improve the Cherenkov detectors. The reason is that in a conventional dielectric medium, the emitted radiation travels in the same direction as the particles, which will interfere with the detection of those photons. However, in metamaterials, photons and charged particles move in opposite directions so that their physical interference is reduced. Though great progress has been made in the past decade on theoretical, numerical and experimental study of reversed CR [66, 104, 123], many challenging issues need to be resolved before the reversed CR can be put in practical applications. Since the intensity of CR increases with frequency, the optical or ultraviolent spectrum is more useful for detection. However, fabrication techniques for creating low loss metamaterials at optical or ultraviolent frequencies [57] is far less mature.

1.2 Governing Equations for Metamaterials

The Maxwell's equations are the fundamental equations for understanding most electromagnetic and optical phenomena. In time domain, the general Maxwell's equations can be written as

$$\text{Faraday's law (1831):} \quad \nabla \times \mathbf{E} = -\frac{\partial \mathbf{B}}{\partial t}, \tag{1.9}$$

$$\text{Ampere's law (1820):} \quad \nabla \times \mathbf{H} = \frac{\partial \mathbf{D}}{\partial t}, \tag{1.10}$$

which are used to describe the relationship between electric field $\mathbf{E}(\mathbf{x}, t)$ and magnetic field $\mathbf{H}(\mathbf{x}, t)$, and the underlying electromagnetic materials can be described by two material parameters: the permittivity ϵ and the permeability μ. In (1.9) and (1.10), we use the electric flux density $\mathbf{D}(\mathbf{x}, t)$ and magnetic flux density $\mathbf{B}(\mathbf{x}, t)$, which are related to the fields $\mathbf{E}$ and $\mathbf{H}$ through the constitutive relations given by

$$\mathbf{D} = \epsilon_0 \mathbf{E} + \mathbf{P} \equiv \epsilon \mathbf{E}, \quad \mathbf{B} = \mu_0 \mathbf{H} + \mathbf{M} \equiv \mu \mathbf{H}, \tag{1.11}$$

where ϵ_0 is the vacuum permittivity, μ_0 is the vacuum permeability, and $\mathbf{P}$ and $\mathbf{M}$ are the induced polarization and magnetization, respectively. Note that $\mathbf{P}$ and $\mathbf{M}$ are

caused by the impinging fields, which can influence the organization of electrical charges and magnetic dipoles in a medium. How big the induced polarization $\mathbf{P}$ and magnetization $\mathbf{M}$ are depends on the particular material involved. For example, in vacuum, $\epsilon = \epsilon_0, \mu = \mu_0$, hence $\mathbf{P} = \mathbf{M} = 0$; while in pure water, $\epsilon = 80\epsilon_0$ and $\mu = \mu_0$, which lead to $\mathbf{P} = 79\epsilon_0\mathbf{E}$ and $\mathbf{M} = 0$.

For metamaterials, the permittivity ϵ and the permeability μ are not just simple constants due to the complicated interaction between electromagnetic fields and meta-atoms (i.e., the unit cell structure). Since the scale of inhomogeneities in a metamaterial is much smaller than the wavelength of interest, the responses of the metamaterial to external fields can be homogenized and are described using effective permittivity and effective permeability. A popular model for metamaterial is the lossy Drude model [311, 313], which in frequency domain is described by:

$$\epsilon(\omega) = \epsilon_0(1 - \frac{\omega_{pe}^2}{\omega(\omega - j\Gamma_e)}) = \epsilon_0\epsilon_r, \tag{1.12}$$

$$\mu(\omega) = \mu_0(1 - \frac{\omega_{pm}^2}{\omega(\omega - j\Gamma_m)}) = \mu_0\mu_r, \tag{1.13}$$

where ω_{pe} and ω_{pm} are the electric and magnetic plasma frequencies, Γ_e and Γ_m are the electric and magnetic damping frequencies, and ω is a general frequency. A simple case for achieving negative refraction index $n = -\sqrt{\epsilon_r\mu_r} = -1$ is to choose $\Gamma_e = \Gamma_m = 0$ and $\omega_{pe} = \omega_{pm} = \sqrt{2}\omega$.

A derivation of (1.12) is given in [235] for very thin metallic wires assembled into a periodic lattice. Assuming that the wires have radius r, and are arranged in a simple cubic lattice with distance a between wires, and σ is the conductivity of the metal, Pendry et al. [235] showed that

$$\omega_{pe}^2 = \frac{2\pi c^2}{a^2 \ln(a/r)}, \quad \Gamma_e = \frac{\epsilon_0 a^2 \omega_{pe}^2}{\pi r^2 \sigma}, \tag{1.14}$$

where c denotes the speed of light in vacuum.

Using a time-harmonic variation of $exp(j\omega t)$, from (1.11) to (1.13) we can obtain the corresponding time domain equations for the polarization $\mathbf{P}$ and the magnetization $\mathbf{M}$ as follows:

$$\frac{\partial^2\mathbf{P}}{\partial t^2} + \Gamma_e\frac{\partial\mathbf{P}}{\partial t} = \epsilon_0\omega_{pe}^2\mathbf{E}, \tag{1.15}$$

$$\frac{\partial^2\mathbf{M}}{\partial t^2} + \Gamma_m\frac{\partial\mathbf{M}}{\partial t} = \mu_0\omega_{pm}^2\mathbf{H}. \tag{1.16}$$

Furthermore, if we denote the induced electric and magnetic currents

$$\mathbf{J} = \frac{\partial\mathbf{P}}{\partial t}, \quad \mathbf{K} = \frac{\partial\mathbf{M}}{\partial t}, \tag{1.17}$$

then we can obtain the governing equations for modeling the wave propagation in a DNG medium described by the Drude model [189]:

$$\epsilon_0 \frac{\partial \mathbf{E}}{\partial t} = \nabla \times \mathbf{H} - \mathbf{J}, \tag{1.18}$$

$$\mu_0 \frac{\partial \mathbf{H}}{\partial t} = -\nabla \times \mathbf{E} - \mathbf{K}, \tag{1.19}$$

$$\frac{1}{\epsilon_0 \omega_{pe}^2} \frac{\partial \mathbf{J}}{\partial t} + \frac{\Gamma_e}{\epsilon_0 \omega_{pe}^2} \mathbf{J} = \mathbf{E}, \tag{1.20}$$

$$\frac{1}{\mu_0 \omega_{pm}^2} \frac{\partial \mathbf{K}}{\partial t} + \frac{\Gamma_m}{\mu_0 \omega_{pm}^2} \mathbf{K} = \mathbf{H}. \tag{1.21}$$

Note that the two-dimensional transverse magnetic model of [311, Eq. (10)] can be obtained directly from (1.18) to (1.21) by assuming that components $E_y, H_x, H_z \neq 0$, while the rest components are 0.

Another popular model used for modeling wave propagation in metamaterials is described by the so-called Lorentz model [259, 269, 313], which in frequency domain is given by

$$\epsilon(\omega) = \epsilon_0 \left(1 - \frac{\omega_{pe}^2}{\omega^2 - \omega_{e0}^2 - j\Gamma_e \omega}\right), \quad \mu(\omega) = \mu_0 \left(1 - \frac{\omega_{pm}^2}{\omega^2 - \omega_{m0}^2 - j\Gamma_m \omega}\right), \tag{1.22}$$

where $\omega_{pe}, \omega_{pm}, \Gamma_e$ and Γ_m have the same meaning as the Drude model. Furthermore, ω_{e0} and ω_{m0} are the electric and magnetic resonance frequencies, respectively.

A derivation of $\mu_r(\omega) = 1 - \frac{F\omega^2}{\omega^2 - \omega_{m0}^2 - j\Gamma_m \omega}$ is shown by Pendry et al. for a composite medium consisting of a square array of cylinders with split ring structure (cf. [236, Fig. 3]) formed by two sheets separated by a distance d. More specifically, they derived

$$\omega_{m0}^2 = \frac{3dc^2}{\pi^2 r^3}, \quad \Gamma_m = \frac{2\sigma}{\mu_0 r}, \quad F = \frac{\pi r^2}{a^2},$$

where the parameters a, c, r and σ have the same meaning as in (1.14). Later, Smith and Kroll [269] changed $F\omega^2$ to $F\omega_0^2$ to ensure that $\mu_r(\omega) \to 1$ as $\omega \to \infty$. This new choice results the Lorentz model (1.22) with $\omega_{pm}^2 = F\omega_0^2$.

Transforming (1.22) into time domain, we obtain the Lorentz model equations for metamaterials:

$$\epsilon_0 \frac{\partial \mathbf{E}}{\partial t} + \frac{\partial \mathbf{P}}{\partial t} - \nabla \times \mathbf{H} = 0, \tag{1.23}$$

$$\mu_0 \frac{\partial \mathbf{H}}{\partial t} + \frac{\partial \mathbf{M}}{\partial t} + \nabla \times \mathbf{E} = 0, \tag{1.24}$$

$$\frac{1}{\epsilon_0\omega_{pe}^2}\frac{\partial^2\mathbf{P}}{\partial t^2}+\frac{\Gamma_e}{\epsilon_0\omega_{pe}^2}\frac{\partial\mathbf{P}}{\partial t}+\frac{\omega_{e0}^2}{\epsilon_0\omega_{pe}^2}\mathbf{P}-\mathbf{E}=0, \tag{1.25}$$

$$\frac{1}{\mu_0\omega_{pm}^2}\frac{\partial^2\mathbf{M}}{\partial t^2}+\frac{\Gamma_m}{\mu_0\omega_{pm}^2}\frac{\partial\mathbf{M}}{\partial t}+\frac{\omega_{m0}^2}{\mu_0\omega_{pm}^2}\mathbf{M}-\mathbf{H}=0. \tag{1.26}$$

The last popular model we want to mention is a mixed model used by engineers and physicists [123, 234, 236, 259, 269], in which the permittivity is described by the Drude model, while the permeability is described by the Lorentz model. More precisely, the permittivity is described by the Drude model [234, 236]:

$$\epsilon(\omega)=\epsilon_0(1-\frac{\omega_p^2}{\omega(\omega+j\nu)}), \tag{1.27}$$

where ω is the excitation angular frequency, $\omega_p > 0$ is the effective plasma frequency, and $\nu \geq 0$ is the loss parameter. On the other hand, the permeability can be described by the Lorentz model [259, 269]:

$$\mu(\omega)=\mu_0(1-\frac{F\omega_0^2}{\omega^2+j\gamma\omega-\omega_0^2}), \tag{1.28}$$

where $\omega_0 > 0$ is the resonant frequency, $\gamma \geq 0$ is the loss parameter, and $F \in (0, 1)$ is a parameter depending on the geometry of the unit cell of the metamaterial.

Using a time-harmonic variation of $exp(j\omega t)$, and substituting (1.27) and (1.28) into (1.11), respectively, we obtain the time-domain equation for the polarization:

$$\frac{\partial^2\mathbf{P}}{\partial t^2}+\nu\frac{\partial\mathbf{P}}{\partial t}=\epsilon_0\omega_p^2\mathbf{E}, \tag{1.29}$$

and the equation for the magnetization:

$$\frac{\partial^2\mathbf{M}}{\partial t^2}+\gamma\frac{\partial\mathbf{M}}{\partial t}+\omega_0^2\mathbf{M}=\mu_0F\omega_0^2\mathbf{H}. \tag{1.30}$$

To facility the mathematical study of the model, by introducing the induced electric current $\mathbf{J}=\frac{\partial\mathbf{P}}{\partial t}$ and magnetic current $\mathbf{K}=\frac{\partial\mathbf{M}}{\partial t}$, we can write the time domain governing equations for the Drude-Lorentz model as following:

$$\epsilon_0\frac{\partial\mathbf{E}}{\partial t}=\nabla\times\mathbf{H}-\mathbf{J}, \tag{1.31}$$

$$\mu_0\frac{\partial\mathbf{H}}{\partial t}=-\nabla\times\mathbf{E}-\mathbf{K}, \tag{1.32}$$

$$\frac{1}{\mu_0\omega_0^2F}\frac{\partial\mathbf{K}}{\partial t}+\frac{\gamma}{\mu_0\omega_0^2F}\mathbf{K}+\frac{1}{\mu_0F}\mathbf{M}=\mathbf{H}, \tag{1.33}$$

$$\frac{1}{\mu_0 F}\frac{\partial \mathbf{M}}{\partial t} = \frac{1}{\mu_0 F}\mathbf{K}, \tag{1.34}$$

$$\frac{1}{\epsilon_0 \omega_p^2}\frac{\partial \mathbf{J}}{\partial t} + \frac{\nu}{\epsilon_0 \omega_p^2}\mathbf{J} = \mathbf{E}. \tag{1.35}$$

In later chapters, we will develop various numerical methods for solving the Drude model (1.18)–(1.21), the Lorentz model (1.23)–(1.26), and the Drude-Lorentz model (1.31)–(1.35).

1.3 A Brief Overview of Computational Electromagnetics

Generally speaking, computational electromagnetics [45] can be classified into either frequency-domain simulation or time-domain simulation. Each category can be further classified into surface-based or volume-based methods. The method of moments (MoM) or boundary element method (BEM) is formulated as integral equations given on the surface of the physical domain. Note that MoM [138] or BEM [55, 56] is applicable to problems for which Green's functions of the underlying partial differential equations are available, which limits its applicability. Hence the volume-based methods such as the finite element method, the finite difference method, the finite volume method (e.g. [76,77,226,239]), and the spectral method (direct applications in computational electromagnetics see [168, 179]; applications in broader areas see [59, 142, 261, 282]) are quite popular.

One of the most favorite methods is the so-called finite-difference time-domain (FDTD) method proposed by Yee in 1966 [299]. Due to its simplicity, the FDTD method is very popular in electrical engineering community, and it is especially useful for broadband simulations, since one single simulation can cover a wide range of frequencies. For more details on the FDTD method, readers can consult Taflove and Hagness' book [276] and references cited therein. This book also provides complete 1-D to 3-D MATLAB source codes so that readers can learn the FDTD method quickly. A recent FDTD book by Hao and Mittra [137] focuses on the simulation of metamaterial models.

But the FDTD method has a major disadvantage when it is used for complex geometry simulation. In this case, the finite element method (FEM) is a better choice as evidenced by several published books in this area. For example, books [267] and [162] focus on how to develop and implement FEMs for solving Maxwell's equations. [267] even provides the Fortran source codes, but it only discusses the standard Lagrange finite elements, which are used to solve the Maxwell's equations written in scalar or vector potentials. Though edge elements are mentioned in this book, no implementation is provided. During 2006 and 2007, Demkowicz et al. published two books [97,98] on hp-adaptive finite element methods for solving both elliptic and time-harmonic Maxwell's equations. Demkowicz also publicized his 2-D Fortran 95 code in [97]. The code implements both rectangular and triangular

edge elements of different orders. In 2008, Hesthaven and Warburton published a very nice package *nudg* in their book [141]. *nudg* has both MATLAB and C++ versions, and can be used to solve the time-dependent Maxwell's equations written in conservation laws. If readers are interested in the finite element theory for Maxwell's equations, the best reference is Monk's book [217]. For a broad coverage on various methods (including FDTD method and FEM) and applications to Maxwell's equations, readers may consult the book by Cohen [85] and the book by Bondeson et al. [42]. However, all those books mentioned above mainly focus on Maxwell's equations in free space, except that [137] is devoted to Maxwell's equations in metamaterials.

In the rest of the book, we will focus on the finite element method due to our experience and interest.

1.4 Bibliographical Remarks

Though the field of metamaterials was born in 2000 [274], it has grown so rapidly that about 20 books (many are edited books) have been published since 2005. For more backgrounds on metamaterials, readers are encouraged to consult them [19, 57, 58, 61, 93, 94, 106, 109, 137, 171, 181, 208–210, 220, 228, 245, 256, 263, 274, 314]. However, they are almost exclusively focused on physics and applications of metamaterials. The only book focused on modeling of metamaterials is [137], which unfortunately covers only finite difference methods.